THE JOURNAL OF PHYSICAL CHEMISTRY C

ARTICLE

pubs.acs.org/JPCC

Effective Medium Properties of Arbitrary Nanoparticle Shapes in a Localized Surface Plasmon Resonance Sensing Layer

Nathan C. Dyck, Ryan C. Denomme, and Patricia M. Nieva*

Department of Mechanical Engineering, University of Waterloo, 200 University Avenue West, Waterloo, Ontario N2L 3G1, Canada

ABSTRACT: Inhomogeneous nanoparticle layers are often modeled as effective homogeneous layers in order to simplify optical device design. Maxwell−Garnett (MG) theory is often used to find the effective medium properties of localized surface plasmon resonance (LSPR) sensing layers. However, MG theory is only applicable for small spherical particles with low filling fractions, thus limiting its applicability. In this paper, an extraction method is used to determine the effective medium properties of an LSPR sensing layer consisting of metal nanoparticles of arbitrary shape. Complex reflection and transmission coefficients (*S* parameters) are found using CST Microwave Studio (CST MWS), a commercial software package. Effective index of refraction (n_{eff}) and impedance (z_{eff}) are calculated from the simulated *S* parameters. This method is extended to account for substrate effects on the effective medium properties. Thus, this method allows for more accurate homogenization of LSPR sensor layers made of any nanoparticle shape, enabling improved LSPR device design.

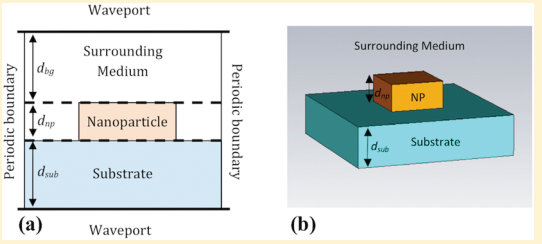

INTRODUCTION

Noble metal nanoparticles have attracted a great deal of attention in the last 10 years as a result of their unique optical properties, specifically, an effect known as localized surface plasmon resonance (LSPR). LSPR is caused by a localized oscillation of a metal nanoparticle's electrons and results in strong electromagnetic scattering and enhanced local fields at the resonance frequency. The resonance frequency is highly sensitive to the nanoparticle's shape,[1] size,[2] chemical composition,[3] and local refractive index.[4] LSPR is useful for enhanced spectroscopy,[5,6] functional layers in optical devices,[7,8] photonic materials,[9,10] and protein biosensing.[1,11−13] In biosensing applications, adsorption events can be detected as a shift in the resonance frequency of the sensor. Therefore, modeling of the LSPR phenomenon is useful for predicting the spectral response of a given nanoparticle conformation, which is invaluable when designing and optimizing LSPR-based sensors. Prediction of the resonance frequency is also useful when designing for functional optical layers, such as in light emitting diodes (LEDs).[7]

The optical response of spherical nanoparticles is well-known and can be described analytically by Mie's theory.[14] Analytical closed form solutions are also available for ellipsoidal nanoparticles.[15] Unfortunately, analytical solutions are not easily found for many other nanoparticle shapes commonly used in LSPR devices. One example of this is the triangular nanoparticles produced by nanosphere lithography[16] (NSL), a low cost fabrication technique used often in LSPR biosensing applications. Developing a flexible model for calculating the optical response of these and other nanoparticle geometries is therefore critical to improving the design of LSPR-based sensors.

Modeling of LSPR-based sensors can be difficult because the nanoparticle sensing layer is heterogeneous. Therefore, it is advantageous to simplify the problem and find effective optical properties for the nanoparticle layer. A common technique used to achieve this is to find the spectral response of a given nanoparticle layer analytically and then use homogenization techniques to transform the heterogeneous nanoparticle layer into an equivalent homogeneous layer with effective optical properties. A homogenization technique used often in the literature for these purposes is the Maxwell−Garnett (MG) theory.[17] In this theory, a relationship is derived to find the effective dielectric constant of a medium containing small spherical inclusions. This theory is widely used for ellipsometry measurements,[18] optical layer design,[7] and biosensor design.[13] MG theory is, however, only valid for low nanoparticle volume filling fractions (<30%),[15] which is defined as the ratio of the volume of the nanoparticles to the volume of the entire layer. This limitation means that coupling between nanoparticles, which affects their plasmonic response,[15] cannot be taken into account; thus dense layers or closely spaced nanoparticles cannot be accurately modeled. In addition, basic MG theory is only valid for small nanoparticle sizes[17] and nanoparticles that are spherical in shape, which limits its applicability to a few special cases. It also cannot take into account the effect of the substrate, which can be significant.[4]

In order to avoid the shortcomings of the MG theory, techniques for effective medium homogenization of arbitrary nanoparticle shapes have been described by Smith et al.[19] for use in metamaterials and by Lidorikis et al.[20] for use in nanoparticle multilayer superstructures. These techniques rely on numerical methods such as the finite-difference time-domain[21] (FDTD)

Received: April 5, 2011
Revised: May 30, 2011
Published: June 20, 2011

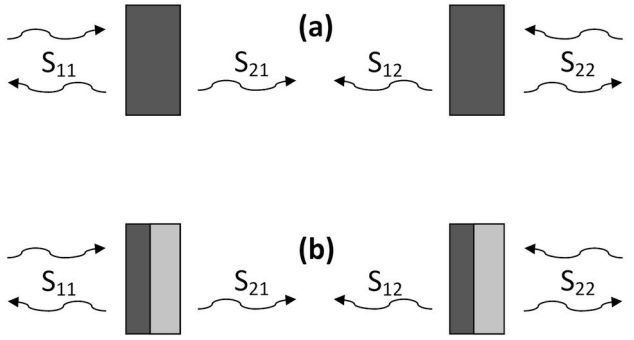

Figure 1. Illustration of the *S* parameters for a (a) symmetric slab and an (b) asymmetric slab, each of which requires slightly different treatment to extract the effective optical properties. Images on the left correspond to light propagation from left to right, while images on the right correspond to light propagation from right to left. S_{11} and S_{22} are the complex reflections for right and left propagation directions, and S_{21} and S_{12} are the complex transmissions for right and left propagation.

method and finite element analysis (FEA) to calculate the optical response of the system. Equations are then employed to extract effective optical properties for an equivalent homogeneous effective medium with the same thickness as the simulated layer. The applicability of these methods is immensely broad and is only limited by the shortcomings of numerical methods and computational power.[22] This work extends these techniques for applications in LSPR-based sensor design. Different nanoparticle shapes are explored as well as the inclusion of substrate effects to create a more accurate and useful model for LSPR sensors. Computer Simulation Technology's Microwave Studio (CST MWS) is used for the optical simulation of the nanoparticle layer. This software provides a 3D CAD environment, which allows any arbitrary shape to be modeled and employs a numerical method known as finite integration technique[23] (FIT). This method is computationally equivalent to FDTD when applied to Cartesian grids in the time domain;[24] however, it relies on discretization of Maxwell's equations in integral form rather than differential form. Homogenization of both symmetric and asymmetric mediums is performed as previously described by Smith et al.[19] and used for subsequent extraction of the effective optical properties.

MODELING METHOD

The technique used for effective optical property extraction presented here is based on the technique described previously by Smith et al.[19] This technique takes the complex reflection and transmission coefficients, also known as scattering parameters (*S* parameters), from numerical simulation and uses them to find the effective refractive index (n_{eff}) and impedance (z_{eff}) of the medium. The *S* parameters are shown schematically in Figure 1. As mentioned, numerical simulations are performed using CST MWS to find the *S* parameters for specified nanoparticle layer geometries. Inputs to these simulations are nanoparticle shape, physical dimensions, orientation, optical material properties for both the nanoparticle material and surrounding medium, boundary conditions such as periodicity, and frequency range of interest. The 3D CAD environment provided by CST MWS can be used to directly specify the geometry of the nanoparticle, which is especially useful for modeling complex 3D shapes. All simulations presented in this paper use CST MWS's frequency domain solver with a tetrahedral mesh.

The retrieval technique presented by Smith et al.[19] allows for homogenization of both symmetric and asymmetric configurations, which are both illustrated in Figure 1. For the case of the symmetric configuration, which is shown in Figure 1a, there is a symmetric optical response, where

$$S_{11} = S_{22} = \text{complex reflection},$$
$$S_{21} = S_{12} = \text{complex transmission} \quad (1)$$

Knowing the thickness of the effective medium, *d*, and the wavenumber (or wavelength, λ) of interest, $k = 2\pi/\lambda$, the simulated *S* parameters can be used to calculate the effective refractive index (n_{eff}) and impedance (z_{eff}) using the equations:[19]

$$n_{eff} = \pm\left(\frac{1}{kd}\cos^{-1}\left[\frac{1}{2S_{21}}\left(1 - S_{11}^{\,2} - S_{21}^{\,2}\right)\right] + \frac{2\pi m}{kd}\right) \quad (2)$$

$$z_{eff} = \pm\left(\frac{(1+S_{11})^2 - S_{21}^{\,2}}{(1-S_{11})^2 - S_{21}^{\,2}}\right)^{1/2} \quad (3)$$

The inverse cosine of eq 2 provides many branches, as indicated by the integer *m*. These branches can lie quite close if *d* is large compared with the wavelength, which can create difficulty in unambiguously determining the effective refractive index. In the case of nanoparticle effective mediums, $d \ll \lambda$, so unambiguous determination of n_{eff} is much more straightforward. For this reason, only the first branch ($m = 0$) is taken and the restriction that $\mathrm{Im}(n_{eff}) > 0$ is imposed to obtain an unambiguous result for the refractive index.[25] Knowing that the layer is a passive material, a further restriction is imposed, which is that $\mathrm{Re}(z_{eff}) > 0$. This allows z_{eff} to also be determined unambiguously. With the effective impedance and refractive index, one can now unambiguously define an effective permittivity (ε_{eff}) and permeability (μ_{eff}) by the following relations

$$\varepsilon_{eff} = \frac{n_{eff}}{z_{eff}}, \quad \mu_{eff} = n_{eff} z_{eff} \quad (4)$$

Asymmetric mediums require a slightly different treatment, as the reflection of a wave propagating in one direction across the medium is not necessarily the same as a wave propagating in the opposite direction. Hence, for the case of the asymmetric configuration, which is shown in Figure 1b, there is an asymmetric optical response, where

$$S_{21} = S_{12}, \quad \text{but} \quad S_{11} \neq S_{22} \quad (5)$$

Consequently, this gives different values for n_{eff} and z_{eff} depending on the direction of propagation. Smith et al. showed that if the unit cell is repeated infinitely, the standard retrieval process for the effective refractive index can be used by employing an averaged *S* parameter,[19]

$$S_{av} = (S_{11}S_{22})^{1/2} \quad (6)$$

The effective refractive index can then be calculated using S_{av} in the place of S_{11} or S_{22} so that eq 2 becomes

$$n_{eff} = \pm\left(\frac{1}{kd}\cos^{-1}\left[\frac{1}{2S_{21}}\left(1 - S_{av}^{\,2} - S_{21}^{\,2}\right)\right] + \frac{2\pi m}{kd}\right) \quad (7)$$

Smith et al.[19] noted that finding an unambiguous effective impedance for an asymmetric medium is not generally possible.

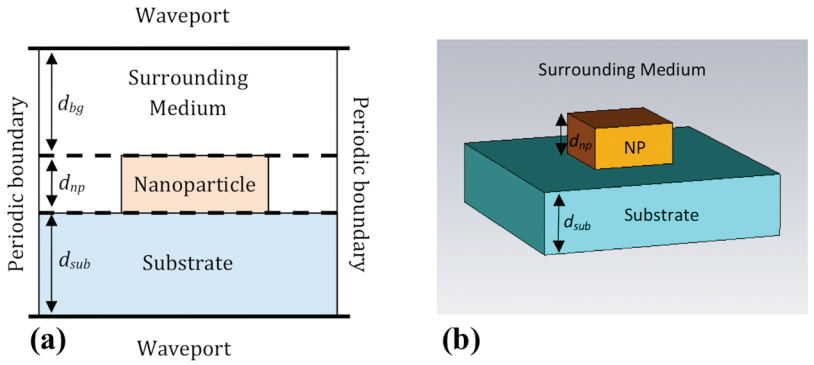

Figure 2. (a) Cross-section schematic and (b) 3D image of CST MWS simulation illustrating the inclusion of substrate effects into the effective optical properties of the nanoparticle layer. The thickness of each of the layers is specified by d_{bg}, d_{np}, and d_{sub}. For illustration purposes, the nanoparticle shown here is a square prism, but any nanoparticle geometry can be modeled. The specific size and shape of the nanoparticles used in this study are detailed subsequently.

The impedance is different depending on the propagation direction and a method does not exist to extract a meaningful averaged impedance. Without an unambiguous result for the impedance, ε_{eff} and μ_{eff} also cannot be defined unambiguously. For this reason, one must compare z_{eff}, ε_{eff}, and μ_{eff} for both the forward and backward propagation directions in the case of an asymmetrical configuration.

The effects of the substrate on the optical properties of the nanoparticles are important to consider because LSPR effects have been shown to be highly dependent on the local refractive index, including the substrates that they are fabricated upon.[4] It has been demonstrated that the LSPR response is dependent on the local refractive index up to 30 nm away from the nanoparticle.[26] Therefore, to accurately determine the effective optical properties of the nanoparticle layer, the substrate must be considered. In this work, the numerical simulations take into account the substrate together with the nanoparticle layer, but only the response of the nanoparticle layer is extracted. This allows the effects of the substrate to be accounted for, while still obtaining the effective properties of only the nanoparticle layer.

A cross-section schematic and a 3D image of the CST MWS simulation, illustrating the inclusion of substrate effects, are shown in panels a and b of Figure 2, respectively. Note that Figure 2 shows a square prism nanoparticle only for illustration purposes, as nanoparticles of any shape or size can be modeled by using the 3D CAD environment. The specific geometries used in this study will be detailed in subsequent sections. To find the effective optical properties for the area indicated between the two dashed lines, d_{np}, periodic boundary conditions are applied to simulate an infinite array of nanoparticles, including the substrate. The waveport size is considered to be at least 30 nm[26] apart from the dashed lines (d_{bg} and d_{sub} for the top and bottom waveports, respectively) to capture as much of the effects of the surrounding refractive index as possible. Because the waveports are placed at a distance away from the layer of interest (the nanoparticle layer), the calculated S parameters have a phase offset that must be accounted for.

Consider a wave propagating from top to bottom in Figure 2. For the retrieval process, the incident phase needs to be 0 at the top dashed line, with the reflected and transmitted phases being measured at the top and bottom dashed lines, respectively. The phase offset can be applied by specifying the "Distance to Reference Plane" in "Waveport Options" within CST MWS, which uses the following two equations

$$S_{11} = S_{11}^{calc}\, exp(-i[kn_{bg}d_{bg} + kn_{bg}d_{bg}]) \quad (8)$$

$$S_{21} = S_{21}^{calc}\, exp(-i[kn_{bg}d_{bg} + kn_{sub}d_{sub}]) \quad (9)$$

where k is the wavenumber, n_{bg}, d_{bg} and n_{sub}, d_{sub} are the refractive index and thickness of the surrounding medium and the substrate, and S_{xx}^{calc} is the S parameter found from the simulation without phase correction applied. Equation 8 gives the phase-corrected S parameters for the reflected waves, and eq 9 gives the phase-corrected S parameters for the transmitted waves. In eq 8, the first term of the exponential accounts for the incident phase offset and the second term accounts for the reflected phase offset. In this case, both terms of the exponential are the same since the reflected wave propagates the same distance, in the same medium (the surroundings), before and after encountering the nanoparticle effective medium. In eq 9, the first term of the exponential accounts for the incident phase offset and the second term accounts for the transmitted phase offset. The two terms in the exponential are not the same in this case since the transmitted wave travels through two different media, the surroundings and the substrate, before and after passing through the nanoparticle effective medium. This correction allows the S parameters to be obtained for the nanoparticle layer alone by removing the phase offset that occurs due to placing the waveports at a finite distance from the nanoparticle layer.

Addition of the substrate also creates an asymmetrical response. For this reason, the asymmetrical retrieval process described by Smith et al., which employs eq 7, must be used. However, this approach will only allow recovery of an effective refractive index for the nanoparticle layer due to ambiguities in the effective impedance, as already discussed.

As a final note, Smith's method is derived for a medium surrounded by vacuum.[19] To account for this, the S parameter results are renormalized to the impedance of free-space ($Z_0 \approx 376.73\ \Omega$) before the effective refractive index is extracted. The renormalization is done within CST MWS by specifying a renormalization impedance when exporting results. However, it can also be accomplished using renormalization procedures outlined elsewhere.[27]

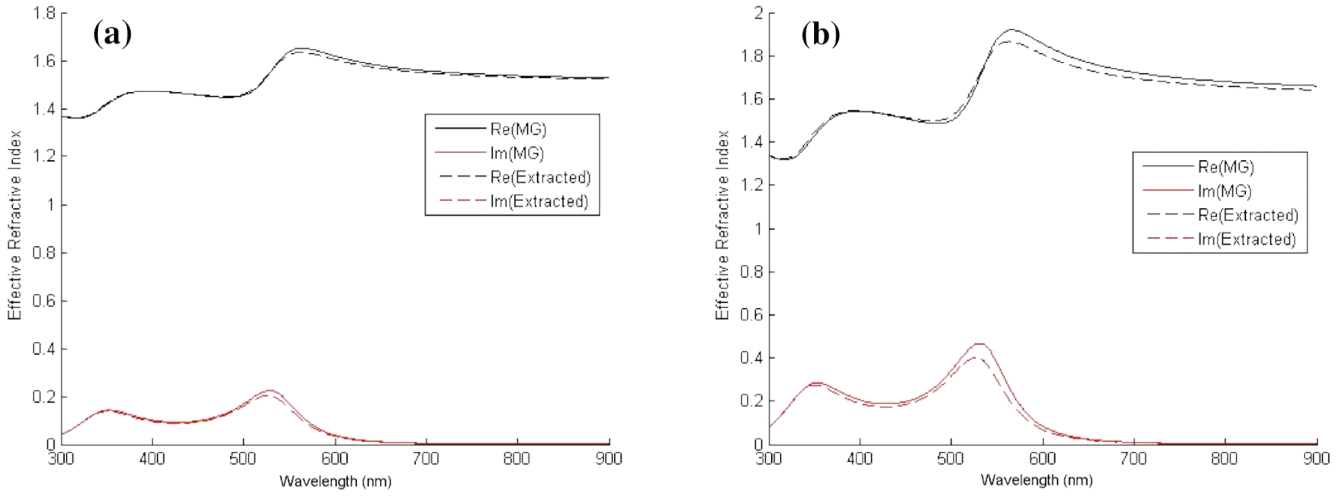

Figure 3. Comparison between CST MWS extraction method and MG theory for finding the effective refractive index of a 10 nm gold nanoparticle layer with volume filling fractions of (a) 5% and (b) 10%. Good agreement is seen between the effective refractive index calculated by each technique, although results begin to deviate at the higher filling fraction. This is likely due to the filling fraction limitations of MG theory, which are not present in the extraction method.

RESULTS AND DISCUSSION

As a first validation of the effectiveness of the extraction method described above, here after called the "extraction method", a single layer of 10 nm spherical gold nanoparticles surrounded by air with various volume filling fractions is simulated and compared to MG results for the same geometry. No substrate is considered in this simulation, making it a symmetric geometry. The scattering parameters of the symmetric medium containing the nanoparticles are determined using CST MWS simulations. In these simulations, the thickness of the effective medium corresponds to the sphere diameter and the periodicity of the unit cell is defined so that the desired nanoparticle filling fractions can be achieved. The effective optical parameters are then calculated using the extraction method, and the results are compared to those obtained using MG theory. For instance, the effective permittivity using MG theory was found using the equation[17]

$$\frac{\varepsilon_{\text{eff}} - \varepsilon_{\text{m}}}{\varepsilon_{\text{eff}} + 2\varepsilon_{\text{m}}} = f\frac{\varepsilon - \varepsilon_m}{\varepsilon + \varepsilon_{\text{m}}} \tag{10}$$

where ε_{eff} is the effective permittivity, ε_{m} is the permittivity of the surrounding medium, ε is the bulk permittivity of the metal inclusions, and f is the volume fraction of spheres in the medium. Because the material is nonmagnetic ($\mu_{\text{eff}} \approx 1$), the effective refractive index can be calculated as $n_{\text{eff}} = (\varepsilon_{\text{eff}})^{1/2}$ and thus compared with the effective refractive index found using the extraction method.

For the purpose of this comparison, gold spheres with a diameter of 10 nm in a surrounding medium of air ($\varepsilon_{\text{m}} = 1.0$) are used. The effective parameters are determined using both methods, for sphere filling fractions of 5% and 10%. For simplicity, the bulk permittivity of gold is approximated by the following Drude−Lorentz model[28]

$$\varepsilon(\omega) = \varepsilon_1 - \frac{{\omega_{\text{p}}}^2}{i\nu_{\text{c}}\omega + \omega^2} + \frac{\varepsilon_{\text{L}}{\omega_0}^2}{{\omega_0}^2 - 2i\delta_0\omega - \omega^2} \tag{11}$$

where $\varepsilon_1 = 7.077$, $\omega_{\text{P}} = 1.391 \times 10^{16}$ rad/s, $\nu_{\text{C}} = 1.411 \times 10^{7}$ rad/s, $\varepsilon_{\text{L}} = 2.323$, $\omega_0 = 4.635 \times 10^{15}$ rad/s, and $\delta_0 = 9.267 \times 10^{14}$ rad/s.

Comparison plots of the real and imaginary parts of the effective refractive index found using each method are presented in Figure 3, showing good agreement between the effective refractive index calculated by both the conventional MG method and the CST MWS extraction method. However, it is clear that at the higher filling fraction the results from the extraction method differ from MG theory. This is most likely because MG theory is only valid for lower filling fractions.[15] These results validate the proposed extraction method at low filling fractions and suggest that this method could be more useful than MG theory for higher filling fractions, since the accuracy of the method described is not dependent on the filling fraction. Also, since the extraction method is not limited to simple spheres, it can be used to calculate the effective optical properties of any nanoparticle shape at any filling fraction.

For the previous simulations, no substrate was considered, so that a direct comparison could be made between the results of the extraction method and MG theory, which does not account for substrate effects. However, a more accurate effective refractive index can be obtained if the substrate is included in the numerical simulations. This is because LSPR effects have been shown to be highly dependent on the local refractive index, including the substrates that they are fabricated upon.[4] Therefore, another useful aspect of the extraction method presented here is the ability to take into account the effect of the substrate on the optical properties of the nanoparticle layer, which is demonstrated below. Substrate effects have been incorporated into effective medium calculations in the past, but nanoparticle geometries are generally restricted to simple shapes, such as spheres[29] and spheroids,[30−32] which is a major limitation. Although the impact of substrates on the optical response of more complex-shaped nanoparticles has been investigated using numerical techniques,[4,33] to the best of the authors' knowledge, none has done so in order to extract the effective optical properties of the nanoparticle layer alone. Knowing the effective optical properties is advantageous for incorporation of the nanoparticle layer into models of practical devices that often have many other optical layers in addition to the nanoparticle layer. Therefore, using the extraction method presented, the effective optical properties of any nanoparticle geometry can

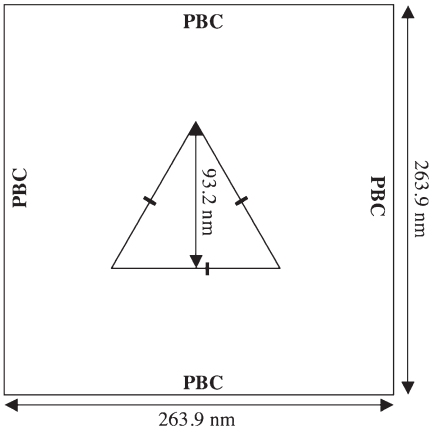

Figure 4. Top-down schematic of the triangular gold nanoparticles used in these simulations to illustrate the effect of the substrate and demonstrate the ability to model complex shapes. The geometry is based on the nanoparticles produced by NSL using 400 nm microspheres. PBC stands for periodic boundary condition.

be readily calculated, while accounting for the effect of the substrate.

To demonstrate the usefulness of taking into account substrate effects, as well as the ability to address more complex nanoparticle shapes, a typical triangular nanoparticle array produced by nanosphere lithography (NSL) is simulated, both with and without the inclusion of a substrate. The triangular nanoparticles are modeled based on the geometry that would result from using 400 nm microspheres as a mask for metal deposition and liftoff. For simplicity, equilateral triangular prisms are modeled, which are a close geometric representation of the truncated tetrahedron shape used to describe nanoparticles resulting from NSL. A top-down view of the nanoparticle is schematically presented in Figure 4 to describe the simulation geometry. The nanoparticles are assumed to be made out of gold and have a thickness of 50 nm.

The triangular nanoparticle has a perpendicular bisector of 93.2 nm and the unit cell has periodicity of 263.9 nm in both the x and y directions, resulting in a filling fraction of 7.2%, which is determined by the NSL fabrication process. Since the nanoparticles are triangular prisms, the filling fraction is only dependent on the particle area and periodicity and not the particle height. It should be noted that application of periodic boundary conditions as seen in Figure 4 results in a square grid arrangement of particles, which is different from the hexagonal arrangement that results from NSL. However, this is not expected to have a large influence on the results since the decay length of the LSPR effect has been shown to be on the order of 30 nm,[26] i.e., an order of magnitude less than the 156.3 nm separation between nanoparticles in this scheme.

The triangular nanoparticles are first simulated without a substrate, in a surrounding medium of air ($\varepsilon_{\text{eff}} = 1.0$). Although the Drude−Lorentz model[28] is usually more convenient to work with, bulk optical constants for gold determined experimentally by Johnson and Christy[34] have been used here to allow a more accurate comparison with experimental results. The symmetric retrieval method (eq 7) is used once the S parameters are found, and the results for refractive index, impedance, permittivity, and permeability are presented in Figure 5. The imaginary part of the effective refractive index of the nanoparticle layer is indicative of optical absorption and is therefore used as an indicator of LSPR. In this case, Figure 5a shows an LSPR peak at 582.7 nm.

The simulation is performed again, using the same configuration in Figure 4 and a cross section as shown in Figure 2, but this time including a substrate of silicon dioxide ($n_{\text{sub}} = 1.46$). The surrounding medium, triangular nanoparticle, and substrate thicknesses are all assumed to be the same and equal to 50 nm. Due to the asymmetry of the configuration, slightly different results are found for z_{eff}, ε_{eff}, and μ_{eff} depending on the direction of propagation. For this reason, the refractive index extracted using the averaged S parameter and eq 7 provides the best option for comparison. The results of these simulations for effective refractive index (using the averaged S parameter), impedance, permittivity, and permeability are presented in Figure 6. Since a single unambiguous value cannot be found for impedance, permeability, or permittivity, results are shown for both propagation directions for these extracted parameters. Figure 6a shows a peak in the imaginary part of the refractive index at 622.2 nm, which is the LSPR peak. This indicates a red shift of 39.5 nm in the LSPR peak position when compared with the results obtained without a substrate. This corresponds to a substrate induced red shift of 86 nm RIU^{-1} (where RIU is refractive index unit), which is on the same order of magnitude as the experimental study done for silver nanoparticles by Malinsky et al.[35] Hence, these results illustrate the need for including substrate effects when attempting to accurately determine the effective optical properties of an LSPR nanoparticle layer, again proving the usefulness of this technique.

It should be noted that in both Figures 5d and 6d a small effective magnetic response is observed near the plasmon resonance frequency. An effective magnetic response from arrays made from nonmagnetic materials is not uncommon and has been observed in left-handed metamaterials[19,25] as well as in nanoparticle superstructures.[20] The magnetic response observed is not necessarily negligible, as seen especially in Figure 6d, and therefore represents an additional advantage of this method over methods such as MG theory, which neglect any magnetic response. This response should therefore be considered when using the extracted optical parameters of the nanoparticle layer.

To further verify the accuracy and usefulness of the extraction method presented here, the response of a real LSPR sensor, previously reported by Hiep et al.,[36] is simulated. Hiep's sensor consisted of an LSPR layer on top of an optical interference layer, which was called an "interference LSPR" (iLSPR) sensor. In Hiep's device, a 500 nm silicon dioxide layer was sandwiched between a gold nanoparticle layer and a silicon substrate. The gold nanoparticle layer was made of 50 nm spherical inclusions at a filling fraction of 21.4%. Hiep used MG theory and multilayer reflectance Fresnel theory to model the sensor. Bulk optical constants of gold, silicon, and silicon dioxide were used for the calculation of the Fresnel coefficients. The RI of the surrounding medium was the same as that of the dielectric film containing dispersed small gold nanoparticles on the SiO_2/Si substrate.[36] Results from the modeling and experiments performed by Hiep for this device within two different mediums, air and oil, are shown in Figure 7.

To model Hiep's sensor using the extraction method, bulk optical constants for gold[34] and silicon[37] are used. Here, the data from Johnson and Christy[34] for the gold optical constants is used once again instead of the Drude−Lorentz model[28] to more accurately compare the results of the extraction method to the experimental results from Hiep. CST MWS is used to find the

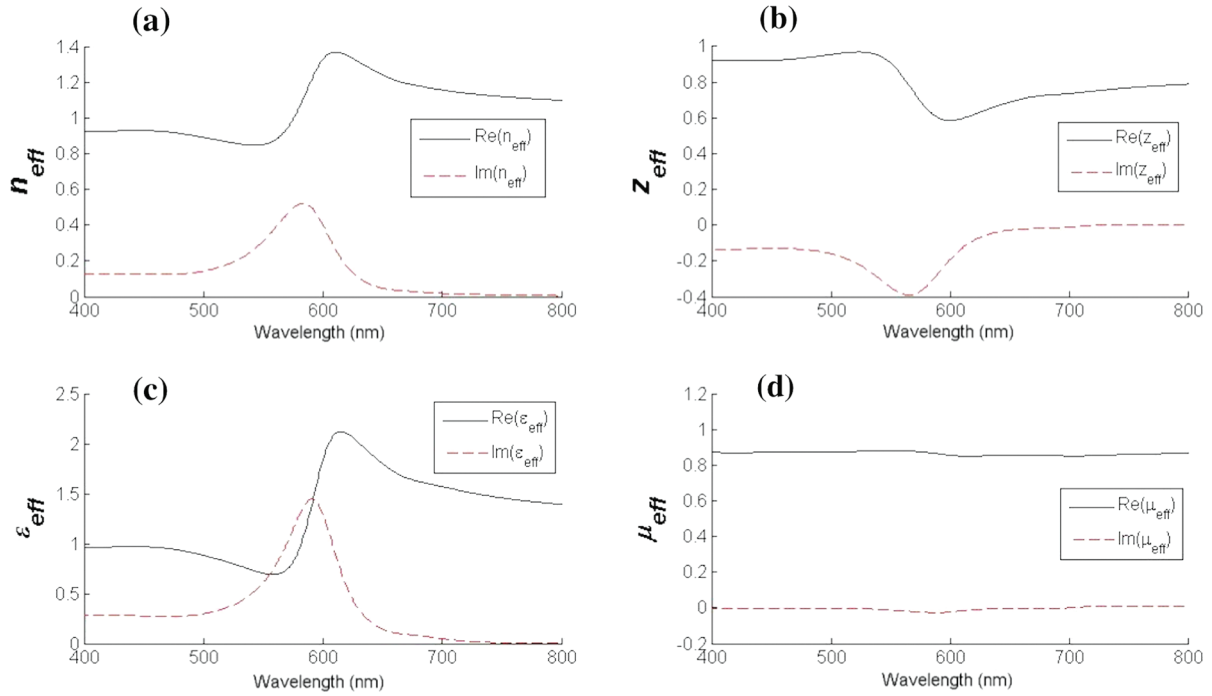

Figure 5. Simulation results for the (a) effective refractive index, n_{eff}, (b) effective impedance, z_{eff}, (c) effective permittivity, ε_{eff}, and (d) effective permeability, μ_{eff}, of the NSL triangular nanoparticle layer extracted from CST MWS simulations. The substrate is not considered, and the LSPR peak is at 582.7 nm.

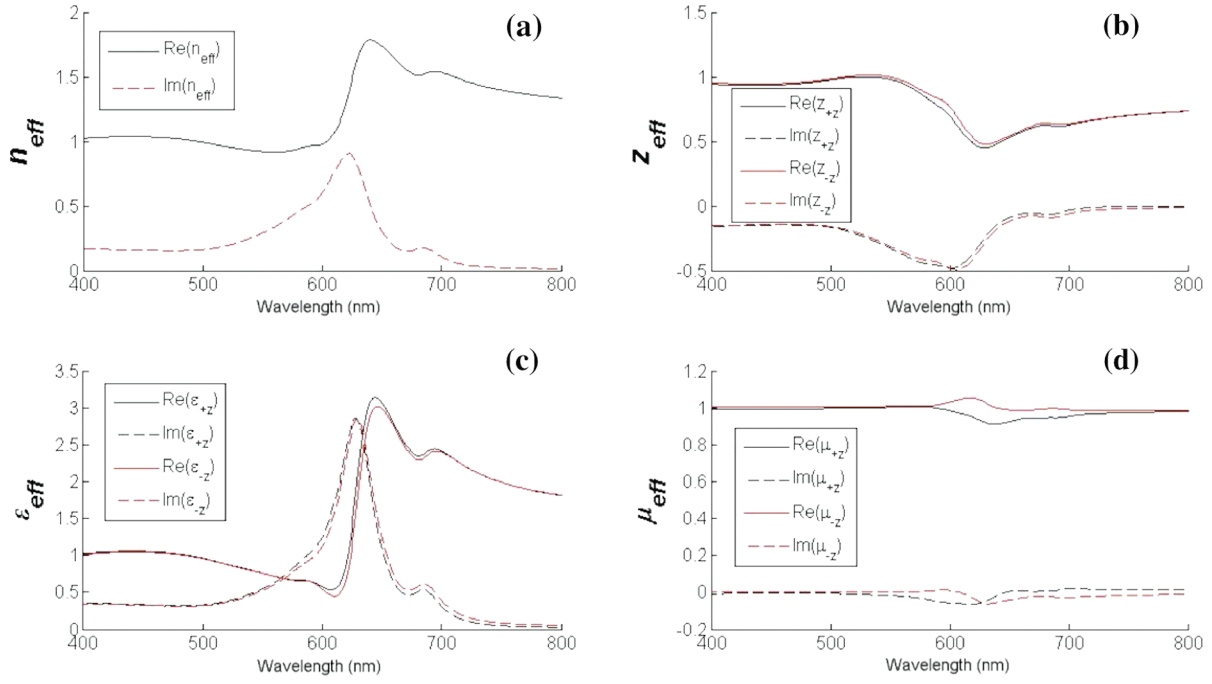

Figure 6. Simulation results for the (a) effective refractive index, n_{eff}, calculated using S_{av} and eq 7, (b) effective impedance, z_{eff}, for forward ($+z$) and reverse ($-z$) propagation directions, (c) effective permittivity, ε_{eff}, for forward ($+z$) and reverse ($-z$) propagation directions, and (d) effective permeability, μ_{eff}, for forward ($+z$) and reverse ($-z$) propagation directions of the NSL triangular nanoparticle layer with substrate (silicon dioxide, n_{sub} = 1.46) effects included. The LSPR peak is at 622.2 nm, indicating a shift of 39.6 nm when compared to the case without a substrate.

effective refractive index of the nanoparticle layer, in air and in oil, using a similar configuration to that shown in Figure 2 with a 50 nm spherical particle sitting on a 30 nm silicon dioxide (n = 1.46) layer. After extraction of the effective refractive index, multilayer Fresnel theory[38] is used to find the overall reflectance of the multilayer sensor system. For simplicity in the multilayer reflectance calculations, the small effective magnetic response observed near resonance is ignored by assuming μ_{eff} = 1. At this

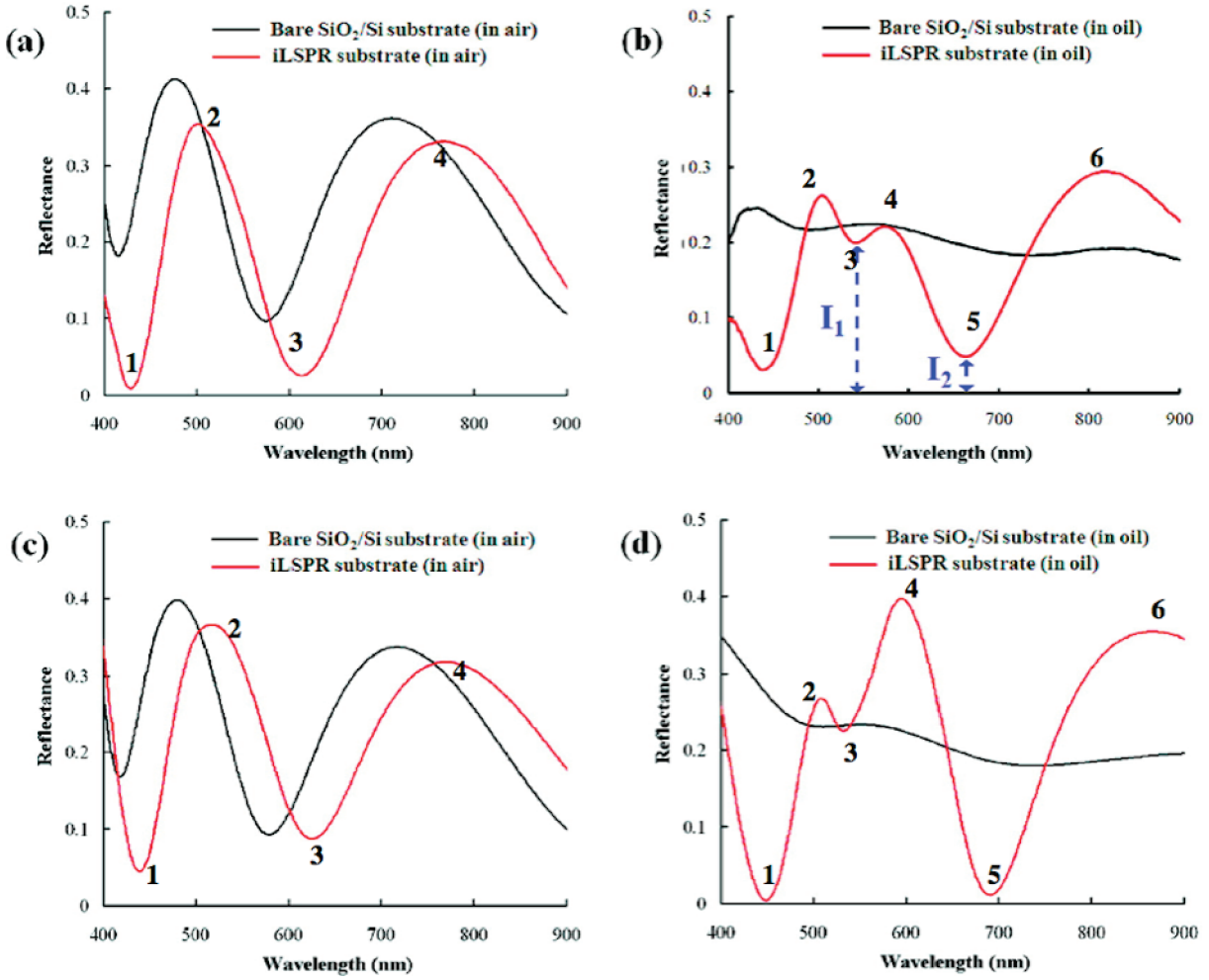

Figure 7. Experimental reflection spectra of bare SiO_2/Si substrate and iLSPR substrate measured in (a) air (n_{air} = 1), and (b) oil (n_{oil} = 1.516). Simulation results of reflection spectra calculated using MG theory, measured (c) in air and (d) in oil.[36]

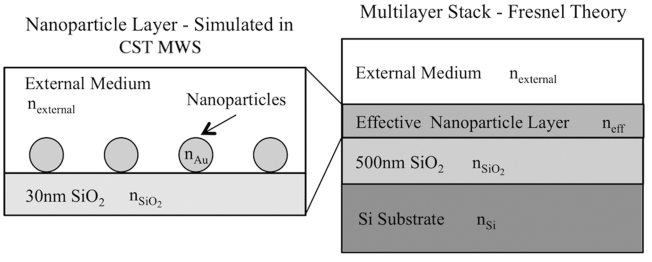

Figure 8. Modeling approach for Hiep's multilayer iLSPR sensor. The nanoparticle layer simulated in CST MWS is illustrated on the left. The multilayer stack solved with Fresnel theory is shown on the right, with the effective nanoparticle layer having properties determined from the CST MWS extraction.

stage, it is not known to what extent this simplification affects the results and further work is needed to assess this in the future. The modeling approach is illustrated in Figure 8. In the Fresnel model, the reflectance is calculated for a 50 nm thick effective nanoparticle layer (using the extracted refractive index), on top of a 500 nm silicon dioxide layer, using air or oil as the external (or entrance) medium and silicon as the exit medium. Results are presented in Figure 9.

To compare Hiep's results with the ones obtained here, the peak and valley positions and reflectance magnitudes are marked in Figures 7 and 9 and summarized in Table 1. The table presents results for peak position as well as reflectance magnitude (in %). It can be observed that the extraction method produces results that more closely match the experimental results presented by Hiep. In general, for the iLSPR sensor in air, similar peak positions from the MG theory and the extraction method are seen, both of which differ slightly from the experimental positions. However, for extreme point 3, in air, the extraction method produces a reflectance (2%) in closer agreement with experimental results (3%) when compared with MG theory (9%). In addition, there is a much better agreement between the reflectance values calculated with the extraction method at extreme points 4 and 6 and the peak position for extreme points 5 and 6. Finally, a much more pronounced difference between the two approaches is seen when considering the oil medium, with the extraction method producing results that agree more closely with the experimental results, in most cases.

It is expected that the larger errors seen between Hiep's simulations and experimental results is mainly due to substrate effects not being considered and the fact that the MG theoretical approach has inherent limitations in accuracy due to both filling

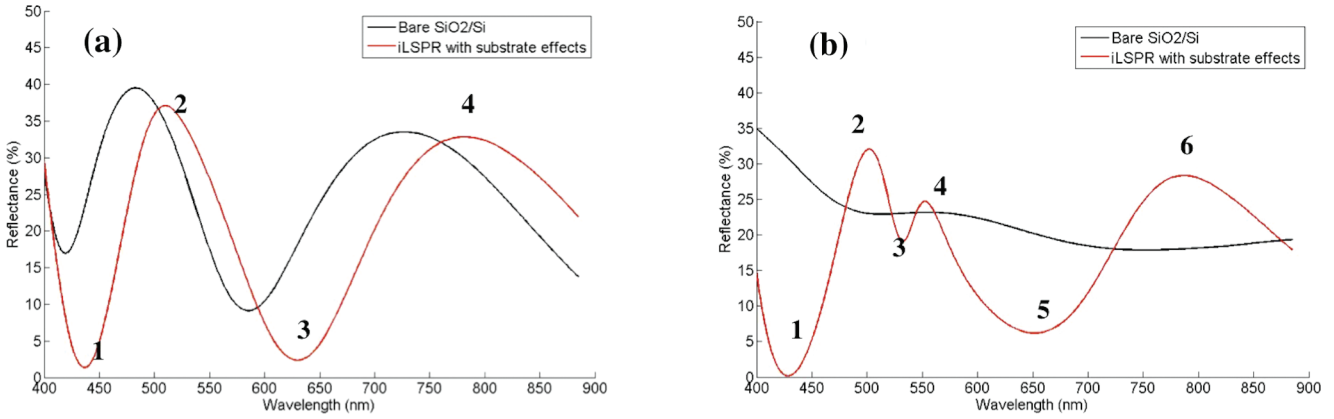

Figure 9. Reflectance spectra calculated in this paper for Hiep's iLSPR sensor using the CST MWS extraction method, including the substrate effects, (a) in air and (b) in oil. Compared to MG theory, the results from the extraction method show better agreement with the experimental results presented by Hiep.

Table 1. Local Extrema Positions and Reflectance Magnitudes Comparing Hiep's Experimental Results with Both Modeling Methods (MG Theory and Extraction Method)[a]

	local extrema	experimental (position, reflectance)	MG theory (position, reflectance)	extraction method (position, reflectance)
air	1	425 nm, 1%	440 nm, 4%	430 nm, 1%
	2	500 nm, 35%	510 nm, 36%	510 nm, 37%
	3	610 nm, 3%	625 nm, 9%	625 nm, 2%
	4	775 nm, 33%	770 nm, 32%	780 nm, 33%
oil	1	430 nm, 3%	450 nm, ~0%	430 nm, ~0%
	2	500 nm, 26%	510 nm, 27%	505 nm, 32%
	3	540 nm, 20%	530 nm, 22%	530 nm, 20%
	4	575 nm, 22%	590 nm, 40%	550 nm, 25%
	5	660 nm, 5%	690 nm, 1%	650 nm, 6%
	6	815 nm, 29%	860 nm, 35%	780 nm, 28%

[a] Local extrema numbers correspond to those marked in Figures 7 and 9. Compared to MG theory, the extraction method produces results that show better agreement with experimental results.

fraction and particle size restrictions.[15] However, although the extraction method produced results closer to the experimental results, there are still differences in peak position and height. It is believed that this is in part caused by the size distribution of the nanoparticles, which was not taken into account. In addition, the nanoparticles in Hiep's device are randomly distributed, while in the simulation, an ordered cubic arrangement was used, thus disregarding some possible interparticle coupling effects. Also, in this case, the small magnetic response observed near the plasmon resonance has been ignored. This could also contribute to the differences in peak height and position.

CONCLUSIONS

A numerical simulation technique has been applied to LSPR devices and extended to include substrate effects, based on the extraction of the effective medium properties (refractive index and impedance) of symmetric and asymmetric nanoparticle arrays with arbitrary geometry. This approach provides considerable versatility compared with analytical approaches such as Maxwell−Garnett theory, which is limited to small spheres and low filling fractions. It allows nanoparticles of arbitrary shape to be examined within the confines of the numerical simulation and computational power. The method also reveals effective magnetic responses, which are ignored when using MG theory. In addition, the approach provides a method to include substrate effects, which are crucial to accurately describing the LSPR effect in practical devices. The method was used to extract the effective refractive index of a nanosphere lithography triangular nanoparticle array on a silicon dioxide substrate. Substrate sensitivity found through simulation was reasonable compared with experimental results from the literature.

The method was further validated by using it to model an iLSPR multilayer sensor configuration. The extracted refractive index was combined with Fresnel theory and used to find the reflectance of a sensor presented by Hiep et al. Results found using the extraction method are in closer agreement with experimental results when compared with simulation results obtained using MG theory, illustrating the effectiveness of this method. Numerical simulations allow the inclusion of specific details, such as substrate properties and nanoparticle shape, physical dimensions, and filling fraction, which significantly affect the LSPR response of a nanoparticle sensing layer. Using the method outlined, effective medium properties can be obtained that account more fully for LSPR effects, thus providing an important tool for the design of LSPR-based sensors and devices.

AUTHOR INFORMATION

Corresponding Author
*E-mail: pnieva@uwaterloo.ca.

ACKNOWLEDGMENT

This research is funded by the Natural Sciences and Engineering Research Council (NSERC) of Canada, the Foothills Research Institute, Early Warning, Inc., and the Ministry of Research and Innovation (MRI) Canada. The authors would like to acknowledge especially fruitful discussions and collaborative work with Professor Matt Vijayan. They would also like to acknowledge the products and services provided by CMC Microsystems (www.cmc.ca) that facilitated this research, including CAD tools.

REFERENCES

(1) Willets, K.; Van Duyne, R. P. *Annu. Rev. Phys. Chem.* **2007**, *58*, 267–297.
(2) Haes, J.; Haynes, C. L.; Van Duyne, R. P. *Mater. Res. Soc. Symp. Proc.* **2001**, *636*, D4.8.1–D4.8.6.
(3) Barbillon, G.; Bijeon, J. L.; Plain, J.; Lamy de la Chapelle, M.; Adam, P. M.; Royer, P. *Surf. Sci.* **2005**, *601*, 5057–5061.
(4) Kelly, K. L.; Coronado, E.; Zhao, L. L.; Schatz, G. C. *J. Phys. Chem. B* **2003**, *107*, 668–677.
(5) Le Ru, E. C.; Etchegoin, P. G. *Principles of Surface-Enhanced Raman Spectroscopy*, 1st ed.; Elsevier: Amsterdam, 2009.
(6) Jensen, T. R.; Van Duyne, R. P.; Johnson, S. A.; Maroni, V. A. *Appl. Spectrosc.* **2000**, *54*, 371–377.
(7) Sung, J. H *Microelectron. Eng.* **2009**, *86*, 1120–1123.
(8) Aziz, H.; Liew, Y. F.; Grandin, M.; Popovic, Z. D. *Appl. Phys. Lett.* **2003**, *83*, 186–188.
(9) Wang, Z.; Chan, C. T.; Zhang, W.; Ming, N.; Sheng, P. *Phys. Rev. B* **2003**, *64*, 113108.
(10) Maier, S. A.; Kik, P. G.; Atwater, H. A.; Meltzer, S.; Harel, E.; Koel, B. E.; Requicha, A. G. *Nat. Mater.* **2003**, *2*, 229–232.
(11) Anker, J.; Hall, W. P.; Lyandres, O.; Shah, N. C.; Zhao, J.; Van Duyne, R. P. *Nat. Mater.* **2008**, *7*, 442–453.
(12) Zhao, J.; Zhang, X.; Yonzon, C.; Haes, A; Van Duyne, R. P. *Nanomedicine* **2006**, *1*, 219–228.
(13) Fu, J.; Park, B.; Zhao, Y. *Sens. Actuators, B* **2009**, *141*, 276–283.
(14) Mie, G. Beiträge zur Optik trüber Medien, speziell kolloidaler Metallösungen. *Ann. Phys.* **1908**, *330*, 377–445.
(15) Myroshnychenko, V.; Rodriguez-Fernandez, I. P.; Funston, A. M.; Novo, C.; Mulvaney, P.; Liz-Marzen, L. M.; Garcia de Abajo, F. J. *Chem. Soc. Rev.* **2008**, *37*, 1792–1805.
(16) Hulteen, J. C.; Van Duyne, R. P. *J. Vac. Sci. Technol., A* **1995**, *13*, 1553–1558.
(17) Garnett, J. C. *Philos. Trans. R. Soc. London, Ser. A* **1904**, *203*, 385–420.
(18) Su, Y. H.; Teoh, L. G.; Lai, W. H.; Chang, S. H.; Yang, H. C.; Hon, M. H. *Appl. Spectrosc.* **2007**, *61*, 1007–1014.
(19) Smith, D. R.; Vier, D. C.; Koschny, T. *Phys. Rev. E* **2005**, *71*, 036617.
(20) Lidorikis, E.; Egusa, S.; Joannopoulos, J. D. *J. Appl. Phys.* **2007**, *101*, 054304.
(21) Yee, K. *IEEE Trans. Antennas Propag.* **1966**, *14*, 302–307.
(22) Parsons, J.; Burrows, C. P.; Sambles, J. R.; Barnes, W. L *J. Mod. Opt.* **2010**, *57*, 356–365.
(23) Weiland, T. *AEU Int. J. Electron. Commun.* **1977**, *31*, 116–120.
(24) Wu, B. I.; Wang, W.; Pacheco, J.; Chen, X. *Prog. Electromagn. Res.* **2005**, *51*, 295–328.
(25) Smith, D. R.; Schultz, S.; Markoš, P.; Soukoulis, C. M. *Phys. Rev. B* **2002**, *65*, 195104.
(26) Haes, A.; Zou, S.; Schatz, G.; Van Duyne, R. P. *J. Phys. Chem. B* **2004**, *108*, 6961–6968.
(27) Pozar, D. M. *Microwave Engineering*, 2nd ed.; John Wiley and Sons Inc., New York, 1998.
(28) Kvasnička, P.; Homola, J. *Biointerphases* **2008**, *3*, FD4–FD11.
(29) Barrera, R. G.; Castillo-Mussot, M.; Monsivais, G.; Villasenõr, P.; Mochán, W. L. *Phys. Rev. B* **1991**, *43*, 13819–12826.
(30) Royer, P.; Goudonnet, J. P.; Warmack, R. J.; Ferrel, T. L. *Phys. Rev. B* **1987**, *35*, 3753–3759.
(31) Valamanesh, M.; Borensztein, Y.; Langlois, C.; Lacaze, E. *J. Phys. Chem. C* **2010**, *115*, 2914–2922.
(32) Wormeester, H.; Kooij, E. S.; Poelsema, B. *Phys. Status Solidi* **2008**, *205*, 756–763.
(33) Futamata, M.; Maruyama, Y.; Ishikawa, M. *J. Phys. Chem. B* **2003**, *107*, 7607–7617.
(34) Johnson, P. B.; Christy, R. W. *Phys. Rev. B* **1972**, *6*, 4370–4379.
(35) Malinsky, M. D.; Kelly, K. L.; Schatz, G. C.; Van Duyne, R. P. *J. Phys. Chem. B* **2001**, *105*, 2343–2350.
(36) Hiep, H. M.; Yoshikawa, H.; Saito, M.; Tamiya, E. *ACS Nano* **2009**, *3*, 446–452.
(37) *Handbook of Optical Constants of Solids*; Palik, E. D., Ed.; Academic Press: San Diego, 1998.
(38) Macleod, H. A. *Thin-Film Optical Filters*, 3rd ed.; Institute of Physics Publishing: London, England, 2001.